Distinct collective states due to trade-off between attractive and repulsive couplings

K. Sathiyadevi,[1] V. K. Chandrasekar,[1,*] D. V. Senthilkumar,[2,*] and M. Lakshmanan[3]

[1]*Centre for Nonlinear Science & Engineering, School of Electrical & Electronics Engineering, SASTRA Deemed University, Thanjavur-613 401, Tamil Nadu, India*

[2]*School of Physics, Indian Institute of Science Education and Research, Thiruvananthapuram-695016, India*

[3]*Centre for Nonlinear Dynamics, School of Physics, Bharathidasan University, Tiruchirappalli-620 024, Tamil Nadu, India*

We investigate the effect of repulsive coupling together with an attractive coupling in a network of nonlocally coupled oscillators. To understand the complex interaction between these two couplings we introduce a control parameter in the repulsive coupling which plays a crucial role in inducing distinct complex collective patterns. In particular, we show the emergence of various cluster chimera death states through a dynamically distinct transition route, namely the oscillatory cluster state and coherent oscillation death state as a function of the repulsive coupling in the presence of the attractive coupling. In the oscillatory cluster state, the oscillators in the network are grouped into two distinct dynamical states of homogeneous and inhomogeneous oscillatory states. Further, the network of coupled oscillators follow the same transition route in the entire coupling range. Depending upon distinct coupling ranges, the system displays different number of clusters in the death state and oscillatory state. We also observe that the number of coherent domains in the oscillatory cluster state exponentially decreases with increase in coupling range and obeys a power-law decay. Additionally, we show analytical stability for observed solitary state, synchronized state, and incoherent oscillation death state.

I. INTRODUCTION

A network of coupled nonlinear dynamical systems manifests itself into a plethora of intriguing collective dynamical behaviors, such as clusters, pattern formation, synchronization, and so on [1]. Among them, oscillation quenching is one of the intriguing phenomena observed in various physical, chemical, and biological systems [2]. The phenomenon of quenching can be further distinguished as (i) amplitude death (AD) and (ii) oscillation death (OD). AD is the stabilization of already existing homogeneous steady state (HSS), which was initially identified due to a large parameter mismatch [3,4], but later observed in identical systems with meanfield diffusive interaction [5] and time delayed coupling [6,7]. In the OD state, the oscillators in the network cease their oscillations under the coupling and populate in at least two inhomogeneous steady states (IHSS). Oscillation death was also initially observed due to parameter mismatch in coupled systems [8]. Later, the phenomenon of quenching of oscillations was shown to emerge even in identical oscillators with time-delayed interactions [9,10] and eventually realized in a variety of couplings, such as dynamic coupling [11], conjugate coupling [12], environmental coupling [13] and in repulsive mean field interactions [14,15]. OD state has also been experimentally observed in chemical oscillators [16], chemical droplets [17], thermokinetic oscillators [18], and electronic circuits [19]. Multicluster OD state was reported recently in an ensemble of globally coupled Josephson junctions [20].

Chimera state, which corresponds to the coexistence of coherent and incoherent domains of oscillations in an identical network, is another emerging phenomenon that is being widely reported both theoretically and experimentally in the recent literature [21–24]. In the recent past, much attention has been paid toward understanding the onset of such chimera states [25–28]. Initially, such states were reported under nonlocal coupling [21,22,24,29], eventually realized even in global coupling [30–32], and in nearest-neighbor couplings [33–36], as chimera states were shown to share strong resemblance to (and can reveal underlying dynamical mechanisms in) many real-world phenomena, such as unihemispheric sleep (i.e., ability of some mammals and birds sleeping with one half of the brain while the other half remains awake) [37], epileptic seizure [38], neuronal bump states [39,40], power grids [41], and social systems [42]. Despite the existence of substantial reports on the OD and the chimera states, both these states were reported as separate dynamical entities until recently [43–47].

In this article, we will unravel the emergence of the fascinating phenomenon of chimera death state, which is characterized by the combined features of chimera and oscillation death state. In the chimera death state, the oscillators in the network segregate into two coexisting domains, wherein one domain neighboring nodes occupy the same branch of the inhomogeneous steady state (spatially coherent OD), while in the other domain neighboring nodes are randomly distributed among the different branches of the inhomogeneous steady state (spatially incoherent OD). The interconnection between the chimera and the oscillation death states was reported by Zakharova *et al.* [43] using a symmetry breaking nonlocal coupling, where the transition from amplitude chimera to chimera death via in-phase synchronized state was reported [43–45]. Recently, distinct types of chimera death states were also reported by Premalatha *et al.* [46]. It was shown that

---

*Corresponding authors:

the presence of nonisochronicity parameter leads to structural changes in the chimera death region giving rise to the existence of different types of chimera death states such as multichimera death state, type-I periodic chimera death (PCD-I) state and type-II periodic chimera death (PCD-II) state [46,47].

In this manuscript, we consider a network of nonlocally coupled van der Pol (vdP) oscillators with combined attractive and repulsive interactions. It is known that the counteracting effects of attractive-repulsive couplings play a predominant role in various chemical and biological processes. For instance, excitation-contraction (EC) coupling was employed in cardiac myocytes [48] and a pair of neurons in the presence of coexisting excitatory (attractive) and inhibitory (repulsive) synaptic couplings was analyzed by Yanagita *et. al* [49]. Further, in the gene regulatory network, positive and negative feedback loops are often used to perform various functions such as bistable switches, oscillators, and excitable devices [50]. Here, we elucidate the emergence of various complex collective patterns due to the combined presence of attractive and repulsive couplings. We begin our analysis with a minimal network of two coupled vdP oscillators and illustrate the onset of oscillation death as a function of the repulsive interaction. Further, we extend our analysis to a network of coupled vdP oscillators with nonlocal attractive-repulsive couplings and demonstrate the emergence of distinct collective dynamics as a function of the strength of the repulsive interaction. In particular, the existence of chimera death preceded by a distinct collective state, namely oscillatory cluster state (OC), will be demonstrated. The oscillatory cluster is characterized by the coexisting homogeneous and inhomogeneous oscillatory states. Finally, we will establish that the chimera death state occurs via the distinct oscillatory cluster state due to the interplay of the nonlocal repulsive and attractive couplings using two-parameter phase diagrams.

The structure of the paper is organized as follows: In Sec. II, we describe our model of a network of nonlocally coupled van der Pol oscillators with combined attractive and repulsive couplings. In Sec. III, we demonstrate the emergence of oscillation death as a function of the repulsive coupling in two coupled van der Pol oscillators. Further, we investigate the emergence of distinct chimera death state via oscillatory cluster state in a network of oscillators in Sec. IV, and we discuss the global dynamical behavior in Sec. V. Finally, we summarize our results in Sec. VI.

II. THE MODEL

We consider a simple, prototype, self-excitatory model of van der Pol (vdP) oscillators which can be constructed experimentally using electronic circuits that mimics the dynamics of the human heart [51,52]. Now, we consider a network of nonlocally coupled van der Pol oscillators with combined attractive and repulsive interactions, whose governing equations are represented as

$$\dot{x}_i = y_i + \frac{\epsilon}{2P} \sum_{j=i-P}^{i+P} (x_j - x_i),$$

$$\dot{y}_i = \alpha(1 - x_i^2) y_i - x_i - \frac{q\epsilon}{2P} \sum_{j=i-P}^{i+P} (y_j - y_i), \quad (1)$$

where, $i = 1, 2, ..., N$. Here, N is the total number of oscillators in the network. In Eq. (1), α is the damping parameter, which manifests itself nearly sinusoidal oscillations for smaller values and relaxation oscillations for larger values. The nonlocal interaction is controlled through the coupling strength ϵ and the coupling range (coupling radius) r, which is defined as P/N, where P corresponds to the total number of neighbors in both the directions of oscillators in the network. Particularly, the repulsive interaction among the oscillators is controlled through the parameter q. Initial conditions for x and y are uniformly distributed between -1.0 to $+1.0$. Runge-Kutta fourth-order integration scheme is used with a time step of 0.01 for all our simulations.

Over the decades several investigations employing van der Pol oscillators have reported distinct dynamical behaviors under a variety of coupling configurations. In particular, among the variety of collective behaviors reported so far in the literature using the coupled vdP oscillators, the phenomena of oscillation death, cluster formation, chimera, and chimera death will be reported in a single framework in the present manuscript. Further, we will also show the existence of chimera death preceded by a distinct collective state, namely oscillatory cluster state (OC). Swing of synchronized state is also observed without nonisochronicity parameter in contrast to the one reported in the literature. Further, systematic bifurcation analysis of different dynamical transitions has also carried out all through the article.

III. EMERGENCE OF OSCILLATION DEATH IN TWO COUPLED VAN DER POL OSCILLATORS

At first, we consider the limiting case of two identical van der Pol oscillators with attractive and repulsive couplings between them. The dynamical transitions of the two coupled vdP oscillator will be analyzed through the bifurcation diagrams (using XPPAUT) depicted in Figs. 1(a) and 1(b). The coupled system Eq. (1) is characterized by the following fixed points: (i) trivial fixed point: (0,0,0,0) and (ii) nontrivial fixed points: $(x_1^*, y_1^*, -x_1^*, -y_1^*)$, where, $x_1^* = -\sqrt{\frac{-1 + \alpha\epsilon + q\epsilon^2}{\alpha\epsilon}}$ and $y_1^* = \epsilon x^*$. The corresponding eigen values are

$$\lambda_{1,2} = \frac{1 - \epsilon^2 \mp \sqrt{1 + \epsilon^2 d_1 - 8\epsilon^3 \tilde{\alpha}}}{2\epsilon},$$

$$\lambda_{3,4} = \frac{1 - q\epsilon^2 \mp \sqrt{1 + \epsilon^2 d_2 - 8\epsilon^3 \tilde{\alpha}}}{2\epsilon}, \quad (2)$$

where $\tilde{\alpha} = \alpha + q\epsilon$, $d_1 = 6 + \epsilon^2$, and $d_2 = 4 - 2q + q^2\epsilon^2$. From an analysis of the above eigen values, we find that a pitchfork bifurcation (PB) occurs at the critical coupling strength $\epsilon_{PB} = \frac{-\alpha + \sqrt{\alpha^2 + 4q}}{2q}$. The unstable inhomogeneous steady state, which emerges through a symmetry breaking pitchfork bifurcation, is stabilized via the Hopf bifurcation point $\epsilon_{HB} = \frac{1}{\sqrt{q}}$, which can be deduced by equating the real parts of the eigen values to zero. Figure 1(a) is depicted for the repulsive coupling $q = 0.3$ as a function of the nonlocal coupling strength ϵ. For feeble values of the repulsive coupling (q), in-phase synchronized state (represented by lines connected by filled circles) is found to be stable in the explored range of ϵ due to the predominant effect of the attractive coupling over the repulsive
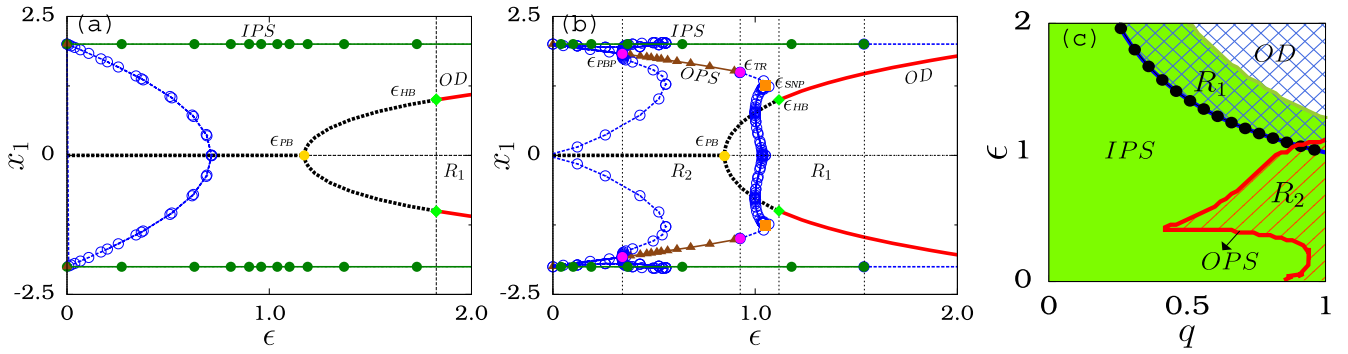
FIG. 1. (a, b) show bifurcation diagrams (using XPPAUT) for $N = 2, \alpha = 0.5$. Panel (a) is plotted for $q = 0.3$ and (b) is for $q = 0.8$. Filled circles (green) and triangles (brown) represent stable IPS and OPS states, respectively. The unfilled circles correspond to unstable OPS. The dotted (black) line and solid (red) line depict unstable and stable nature of steady states. TR, PB, and HB denote torus, pitchfork, and Hopf bifurcation points, respectively. PBP and SNP denote the pitch fork and saddle node bifurcations of periodic orbits. (c) Phase diagram in (q, ϵ) space. R_1 and R_2 are the multistability regions of IPS-OD and IPS-OPS, respectively.

coupling. Dotted line connected by unfilled circles correspond to unstable out-of-phase synchronized state. By increasing ϵ from zero, an unstable inhomogeneous steady state (indicated by broken lines) emerges via pitchfork bifurcation at $\epsilon_{PB} = 1.18$ and is stabilized through a Hopf bifurcation at $\epsilon_{HB} = 1.82$ thereby rendering the stable IHSS (denoted by solid red lines) to coexist with stable IPS state in the region R_1 in Fig. 1(a).

Now, we increase the strength of the repulsive coupling to $q = 0.8$. The dynamical transitions as a function of the nonlocal coupling for $q = 0.8$ are depicted in the bifurcation diagram in Fig. 1(b). It is evident that for smaller values of ϵ, the stable IPS oscillations (lines connected by filled circles) coexist with unstable out-of-phase synchronized (OPS) oscillations (lines connected by unfilled circles). Upon increasing ϵ further, the trade-off between the attractive and repulsive couplings result in the stabilization of the unstable OPS via a pitchfork bifurcation of periodic orbit (PBP) at $\epsilon_{PBP} = 0.344$ leading to bistability between the stable IPS and stable OPS (indicated by lines connected by filled triangles) states in the region R_2. The phase difference between the OPS state is found to be π and hence it may also be regarded as antiphase synchronization. By increasing the coupling strength further results in destabilization of stable OPS states via torus (TR) bifurcation at $\epsilon_{TR} = 0.926$. Further, the saddle-node bifurcation (SNP) of periodic orbits occurs at $\epsilon_{SNP} = 1.04$, shown by a pair of squares in Fig. 1(b), where the unstable quasiperiodic and periodic oscillations collide and disappear leading to monostable limit cycle oscillation (IPS state) in a narrow range of $\epsilon \in (0.926, 1.12)$. In addition, the unstable inhomogeneous steady state that emerges at $\epsilon_{PB} = 0.845$ is stabilized via the Hopf bifurcation at $\epsilon_{HB} = 1.12$ resulting in bistability between IPS and OD state in the region R_1. The coupled system settles at the stable OD state for strong nonlocal coupling as evident from Fig. 1(b).

To observe the role of the repulsive coupling in inducing the oscillation death in the simplest network of two coupled vdP oscillators, we have plotted the two phase diagram in (q, ϵ) space in Fig. 1(c). It elucidates that the coupled system exhibits only IPS state in the entire range of ϵ for lower values of the repulsive coupling strength q. At strong coupling limits competition among the attractive and the repulsive interactions

leads to stable OD state. Moreover, we find bistability between IPS-OPS and IPS-OD in the R_1 and R_2 regions, respectively, in Fig. 1(c). From the above analysis we find that a strong competition between the attractive and repulsive interactions can give rise to the onset of oscillation death. It is also to be noted that the OD state emerges only for larger repulsive coupling strengths. Linear stability analysis shows that the OD state is stable in the region $\epsilon_{HB} > \frac{1}{\sqrt{q}}$ for $q \leqslant 1$ where the stabilization occurs through the Hopf bifurcation. The analytical critical stability curve across which a switch in the stability of unstable inhomogeneous steady state occurs as function of q is represented by the line connected by filled circles in Fig. 1(c). To study the role of the repulsive coupling in inducing various other collective dynamics and the transition to chimera death state via the oscillatory cluster state we extend our analysis to a network of vdP oscillators with nonlocal attractive and repulsive couplings.

IV. ROLE OF REPULSIVE INTERACTION IN A LARGER NETWORK OF OSCILLATORS

In this section we study the effect of nonlocal repulsive coupling together with an attractive coupling in a network of oscillators with $N = 100$ for the nonlocal coupling radius $r = 0.3$.

A. Swing of synchronized states

For the repulsive coupling strength $q = 0.5$, we have found a swing like behavior of synchronized states as a function of ϵ (see Fig. 2). The coupled system exhibits stable synchronized oscillations for smaller values of ϵ, the corresponding snapshot and phase portrait of which are shown in Figs. 2(a) and 2(b) for $\epsilon = 0.1$. The solid (red) line represents the phase portrait of globally synchronized oscillators whereas the filled circle points (black) connecting by the continuous line denote the phase portrait of uncoupled vdP oscillators and it is evident from the figures that the globally synchronized oscillators follow the original trajectory of the uncoupled vdP oscillators.

By increasing ϵ further, stable solitary state emerges as a result of destabilization of the globally synchronized state, as illustrated in Figs. 2(c) and 2(d) for $\epsilon = 0.26$. From the figure, it is clear that the symmetry of the coupled system is broken
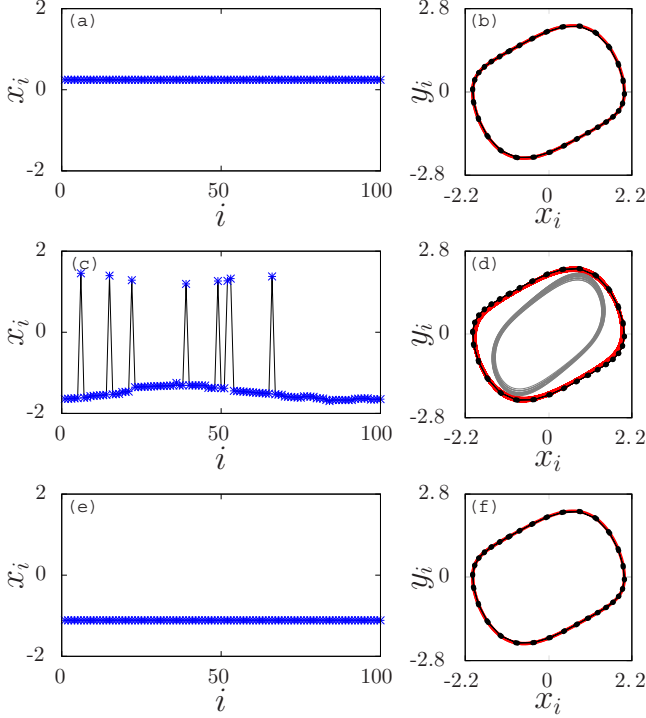
FIG. 2. Snapshots for the variables x_i and phase portraits of the system at $\alpha = 0.5$, $q = 0.5$. (a, b) synchronization (SYN) for $\epsilon = 0.1$, (c, d) solitary state (SS) for $\epsilon = 0.26$, and (e, d) synchronization (SYN) for $\epsilon = 0.6$. The filled circles (black) connected by continuous line represent phase trajectory of the uncoupled oscillator.

spontaneously upon increasing the coupling strength resulting in two different groups comprising of coherent and solitary oscillators. The coherent oscillators (indicated by continuous red line) oscillate about the origin like the uncoupled oscillators whereas the solitary oscillators (indicated by solid gray line) oscillate with different amplitudes. Further increase in ϵ leads to a stabilization of completely synchronized state [see Fig. 2(e)] for $\epsilon = 0.6$ and it follows the same trajectory as that of the uncoupled oscillators. Thus, we have observed a swing of the synchronized state, which was destabilized by the emergence of solitary state and again stabilized as a function of the coupling strength ϵ. It is to be noted that the coherent oscillators always evolve with the same amplitude and frequency as that of the uncoupled oscillator. To characterize the observed dynamical transition, we have estimated the standard deviation as used by Daido and Nakanishi [53] and Premalatha *et al.* [47] using the formula

$$\sigma = \langle (\overline{|x_i - \overline{x_i}|^2})^{1/2} \rangle_t, \qquad (3)$$

where the bar represents the ensemble average and $< \cdot >_t$ represents the time average. The standard deviation is depicted in Fig. 3(a) as a function of the nonlocal attractive coupling ϵ. From Fig. 3(a), it is evident that σ takes null value for the synchronized state and nonzero value for the solitary state thereby corroborating the re-emergence of the stable synchronized state after the emergence of solitary state in a short range of ϵ. It is to be noted that nonisochronicity induced swing of synchronized state was reported in Refs. [47,53], whereas,
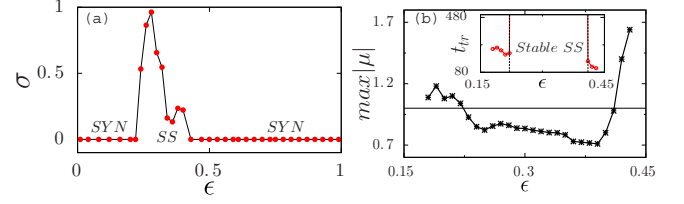

FIG. 3. (a) Standard deviation (σ) at $\alpha = 0.5$, $q = 0.5$ by varying coupling strength ϵ, the null value of the standard deviation stands for synchronized state and nonzero values correspond to the solitary state and (b) maximum Floquet exponent for solitary state. $\max|\mu| < 1$ represents stable solution of periodic orbits and $\max|\mu| > 1$ indicates the unstable nature of the corresponding dynamical state. The corresponding transient behavior is shown in the inset.

in contrast, we have observed the swing of the synchronized state as a function of the nonlocal coupling strength in the presence of the repulsive coupling without introducing any nonisochronicity parameter. As the oscillations in the solitary states are periodic and they are of same frequency, we can find the stability of these states using Floquet theory. For this purpose, we have perturbed Eq. (1) in the form $x_i = x_i^* + \eta_i$ and $y_i = y_i^* + \zeta_i$ and derived the equations

$$\dot{\eta}_i = \zeta_i + \frac{\epsilon}{2P} \sum_{j=i-P}^{i+P} (\eta_j - \eta_i),$$

$$\dot{\zeta}_i = \alpha(1 - x_i^{*2})\zeta_i - (1 + 2x_i^* y_i^*)\eta_i - \frac{q\epsilon}{2P} \sum_{j=i-P}^{i+P} (\zeta_j - \zeta_i),$$

$$(4)$$

where x_i^* and y_i^* correspond to the solitary state and η_i and ζ_i are the perturbation terms. The stability of the periodic orbits can be determined from the values of the Floquet multipliers (μ_i, $i = 1, 2, ... N$). Whenever η_i and ζ_i asymptotically approach zero or finite values, all the Floquet multipliers μ_i's should lie within a unit circle in the complex plane (or $|\mu_i| < 1$). Usually one of the values of μ_i can take the value 1, which is referred to as Goldstone mode in the literature. In such situations, the periodic orbit is stable. If any one of the μ_i's is greater than one, the functions η_i and ζ_i are found to grow up and consequently the periodic orbits are not stable. We have plotted the maximum value of Floquet exponents ($\max|\mu_i|$) as a function of the coupling strength ϵ in Fig. 3(b). It is clear that the value of $\max|\mu| < 1$ shows stable region of solitary state and $\max|\mu| > 1$ indicates the unstable region. The corresponding transient behavior is shown in the inset of Fig. 3(b), which clearly depicts that the values of the Floquet exponents increase with decreasing transient time. In the stable solitary state the system experiences a very large transient time than the unstable region where the transient solitary state exists only for a finite time.

B. Quasiperiodic chimera

A slight increase in q, breaks the system symmetry spontaneously thereby rendering one group of oscillators to the coherent region and the other group of oscillators to the incoherent state leading to the genesis of the fascinating hybrid
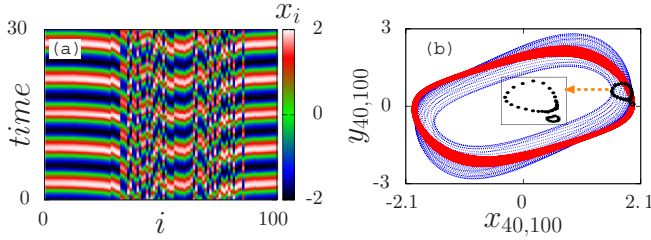
FIG. 4. (a) Space-time plot of the chimera state at $\alpha = 0.5$, $\epsilon = 0.3$, and $q = 0.77$. Panel (b) shows the phase portrait of representative oscillators from the coherent and incoherent groups. The red trajectory corresponds to the representative oscillator (x_{100}, y_{100}) from the coherent group and that from the incoherent group (x_{40}, y_{40}) is represented by blue trajectory. The corresponding Poincaré points are shown on the phase portrait trajectory with filled circles and star points. The closed loop of the Poincaré points confirms the quasiperiodic nature of chimera state.

state of chimera (CM). The space-time plot and phase portraits of quasiperiodic chimera state for $\alpha = 0.5$, $\epsilon = 0.3$, and $q = 0.77$ are illustrated in Figs. 4(a) and 4(b). The oscillators are found to exhibit quasiperiodic oscillations in both coherent and incoherent regions. Representative oscillators from both the groups are shown in Fig. 4(b). Dotted (blue) and solid (red) lines correspond to the oscillator x_{100} from the coherent group and x_{40} from the incoherent group, respectively. The Poincaré points (filled circles and star points) are depicted on the phase trajectory to corroborate that their closed loop structure which signify the quasiperiodic nature of oscillations in the chimera state. The enlarged image of the Poincaré trajectory is shown in Fig. 4(b).

C. Collective dynamics at maximum repulsive coupling ($q = 1$)

In this section, we study the dynamics at the maximum repulsive coupling strength ($q = 1$). Space-time plots and the corresponding frequencies f_i are depicted in Fig. 5 for $\alpha = 0.5$ as a function of the nonlocal coupling strength ϵ. The coupled oscillator network evolves independently resulting in desynchronization-I (DS-I) state for $\epsilon = 0.05$ [see Figs. 5(a) and 5(b)]. In this case, the competition between the attractive and the repulsive interactions leads to the desynchronized state with same amplitude and frequency but with different phases [see Fig. 5(a)]. The phases of the oscillators (even though they oscillate with same frequency) are distributed randomly between zero and 2π. The inset in Fig. 5(b) shows the snapshot image of DS-I state. By increasing ϵ, we observe that the oscillators in the desynchronized group align spontaneously with constant velocity and form a stable coherent traveling wave (TW) as depicted in Figs. 5(c) and 5(d) for $\epsilon = 0.5$. In contrast to the desynchronized state, we find that the oscillators evolve with constant phase differences distributed between zero and 2π as depicted in the inset of Fig. 5(d). Further increase in ϵ leads to strong competition between the attractive and the repulsive nonlocal couplings resulting in desynchronized state (DS-II) as shown in Figs. 5(e) and 5(f) for $\epsilon = 0.92$. The amplitude, phase and frequency of all the oscillators are found to evolve independently as is evident from
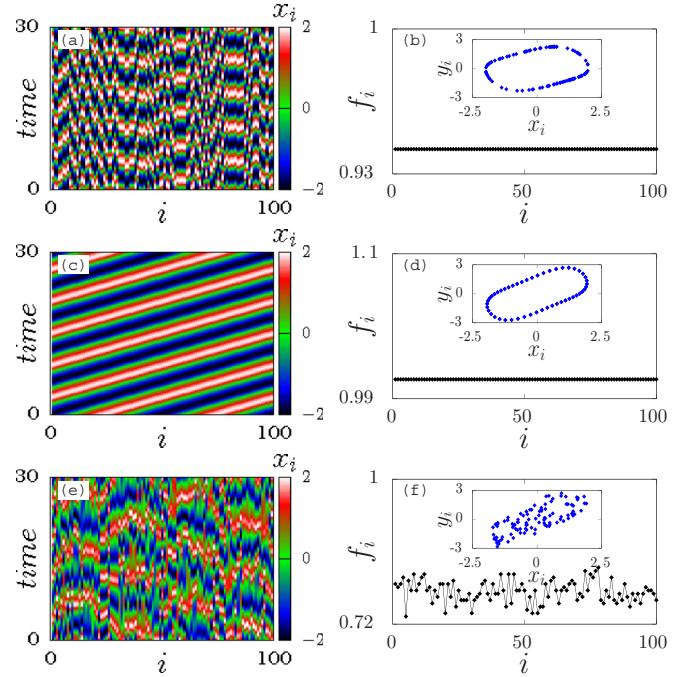

FIG. 5. Space-time plots and the corresponding frequencies f_i for (a, b) desynchronization-I (DS-I) at $\epsilon = 0.05$, (c, d) traveling wave (TW) at $\epsilon = 0.5$, and (e, f) desynchronization-II (DS-II) at $\epsilon = 0.92$. Other parameters are $\alpha = 0.5$ and $q = 1$.

Figs. 5(e) and 5(f). The inset in Fig. 5(f) shows the snapshot of completely desynchronized state.

Splitting of the desynchronized oscillators into homogeneous and inhomogeneous ones facilitating the onset of oscillatory clusters (clusters of different oscillatory states) was observed for further increase in the strength of the nonlocal coupling ϵ. The spatiotemporal plot of an oscillatory cluster (OC) is depicted in Fig. 6(a). To differentiate the domains of homogeneous and inhomogeneous states we have calculated the center of mass using the formula $x_{c.m.} = \int_0^T \frac{x_i(t)dt}{T}$, where $T = \frac{2\pi}{\omega}$ is the period of oscillation. The center of mass of each oscillator is depicted in Fig. 6(b), where the stars represent inhomogeneous oscillations and the unfilled triangles denote the homogeneous oscillations. From the center of mass analysis, it is clear that the homogeneous oscillations always oscillate about the origin characterized by null value of the center of mass whereas the inhomogeneous states take the center of mass away from the origin characterized by nonzero values of the center of mass. We have depicted the phase portraits of homogeneous and inhomogeneous oscillators in the oscillatory clusters in Fig. 6(c) and the enlarged images of inhomogeneous groups are shown in the inset. It is evident that the homogeneous group oscillates with larger amplitudes [represented by dashed lines in Fig. 6(c)] than the inhomogeneous group (solid lines). Further the inhomogeneous group contains more number of oscillators than the homogeneous group. Increasing ϵ further, the number of oscillators in the homogeneous group decreases thereby leading to an increase in the number of oscillators in the inhomogeneous oscillatory group and finally ending up with only a stable inhomogeneous steady state in the strong coupling limit. The space-time and
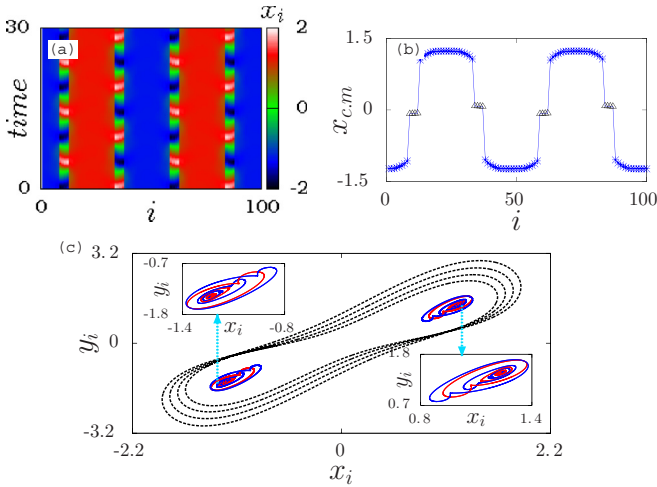
FIG. 6. (a) Space-time plot depicting the oscillatory cluster (OC) state for $\alpha = 0.5, \epsilon = 0.95$ and $q = 1.0$. Center of mass of each oscillator is shown in (b). Here, the center of mass is calculated by averaging over one period of each oscillator. Center of mass of homogeneous oscillations are denoted by unfilled triangles and star represents the oscillators in the inhomogeneous group. (c) Phase portrait of representative oscillators from homogeneous and inhomogeneous group of oscillators. Enlarged images of the inhomogeneous oscillators are shown in the insets.

snapshot images of two coherent cluster steady states (2C-OD) are depicted in Figs. 7(a) and 7(b) for $\epsilon = 1.05$. The oscillators in the coherent edges moves randomly between the upper and the lower branches of the IHSS for further larger ϵ resulting in two cluster chimera death (2C-CD) state as shown in Figs. 7(c) and 7(d). While increasing the strength of the coupling beyond
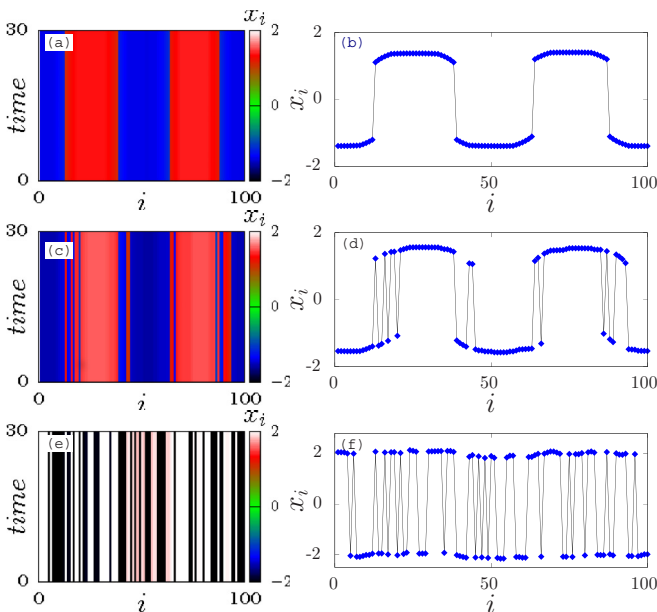

FIG. 7. Space-time and snapshot images for $\alpha = 0.5$ and q=1. (a) Two cluster oscillation death (2C-OD) for $\epsilon = 1.05$, (b) two cluster chimera death (2C-CD) for $\epsilon = 1.18$, and (c) multicluster chimera death (MCD) for $\epsilon = 2.0$.
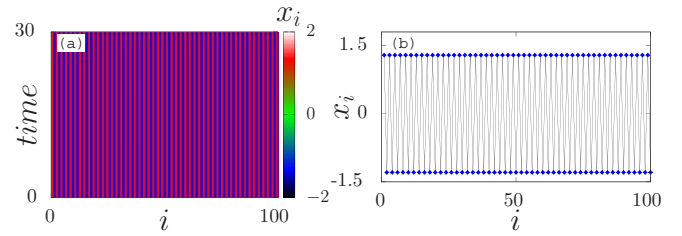

FIG. 8. Space-time and snapshot images of incoherent oscillation death (IOD) state for $\alpha = 0.5$, $q = 1$, and $\epsilon = 2.0$,

$\epsilon = 1.2$, stable multichimera death state (MCD) emerges from 2C-CD [see Figs. 7(e) and 7(f)].

Stable incoherent oscillation death (IOD) state was also found to coexist in the region of stable chimera death state upon distributing the initial state of the oscillators at nearly incoherent oscillation death state. The space-time and snapshot images of IOD state is shown in Figs. 8(a) and 8(b) for $\epsilon = 2.0$. In this state, the oscillators occupy the upper and the lower branches of inhomogeneous steady state alternately as depicted in Fig. 8(b). Thus, it is evident that the trade-off between the repulsive and attractive nonlocal couplings facilitates the onset of a rich variety of collective dynamics in a network of vdP oscillators. In particular, the competing effects between both the couplings lead to a new transition route to the chimera death state, namely oscillatory cluster state. In the earlier reports, the chimera death was observed through a transition from amplitude chimera to chimera death via in-phase synchronized state for lower range of coupling strengths and a direct transition from amplitude chimera to chimera death was reported at larger coupling strengths. The transition routes were reported with respect to coupling range (r) [43]. The amplitude chimera dynamics consists of coherent homogeneous and incoherent inhomogeneous oscillations. The inhomogeneous oscillations in the incoherent state occupy upper and lower branches alternately with different amplitudes. Instead, here the chimera death is observed through oscillatory cluster state with respect to the strength of repulsive coupling q. Here, both homogeneous and inhomogeneous oscillations are in the form of clusters. Moreover, the amplitude chimera dynamics was reported as transient in the previous reports whereas in this work the oscillatory cluster dynamics is found to be stable in all the range of coupling radius [45]. The emergence of oscillatory cluster as a function of the coupling range r and the strength of nonlocal repulsive coupling ϵ will be discussed in the following section.

D. Oscillatory cluster state with respect to *q* and *r*

To understand the robustness of OC state with respect to the coupling range r, we have depicted the number of coherent clusters (homogeneous oscillatory states) in the (q,r) plane in Fig. 9 for a fixed value of $\epsilon = 0.97$. It is evident from the figure that the oscillatory cluster states emerge only above a critical coupling strength of the repulsive interaction. Different symbols attribute to distinct number of oscillatory clusters with respect to the nonlocal coupling radius r. It is also clear that the number of coherent clusters decreases while their spread increases as a function of the coupling range r.
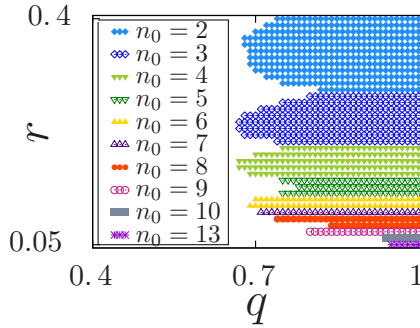
FIG. 9. (a) The number of clusters (coherent domains) of oscillatory cluster state in (q,r) plane for coupling strength $\epsilon = 0.97$ and $\alpha = 0.5$.

There is an exponential decrease in the number of coherent clusters in the oscillatory cluster state as depicted in Fig. 10 for $N = 500$. The inset in Fig. 10 represents log-log plot illustrating that the number of coherent domains obeying the power law $n_0 = ar^b$ with respect to coupling range r. We have also found best fit for $a = 0.802725$ and $b = -0.913692$, which is represented by the red solid line while the corresponding numerical data is represented by the unfilled circles in Fig. 10.

V. GLOBAL DYNAMICAL BEHAVIOR WITH RESPECT TO THE STRENGTH OF THE REPULSIVE COUPLING Q

To understand the global dynamical behavior of the network of coupled vdP oscillators as a function of the strength of the repulsive coupling q and coupling strength ϵ, we have plotted the two parameter plot in (q,ϵ) space for four distinct coupling radius values $r = 0.1$, $r = 0.2$, $r = 0.3$, and $r = 0.4$ in Fig. 11. Traveling wave (TW) and completely synchronized oscillations (SYN) emerge alternately for lower values of q and ϵ [see Fig. 11(a)] for the coupling radius $r = 0.1$. Increasing ϵ for lower values of q results only in completely synchronized state. Solitary state (SS), chimera (CM) and traveling wave (TW) state emerges as a function of q for $\epsilon < 1$ and OD state emerges for larger values of ϵ ($\epsilon > 1$). For the strength of the repulsive coupling $q = 1$, desynchronized state (DS-I)
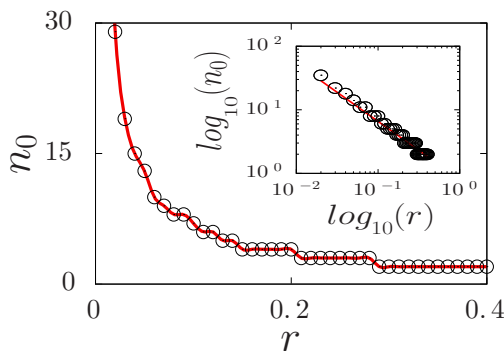

FIG. 10. Exponentially decreasing number of clusters with respect to coupling range for $N = 500$. The corresponding power law fit is shown in the inset with logarithmic scale. Unfilled circles represent the numerical data and the corresponding best fit is shown by red solid line.
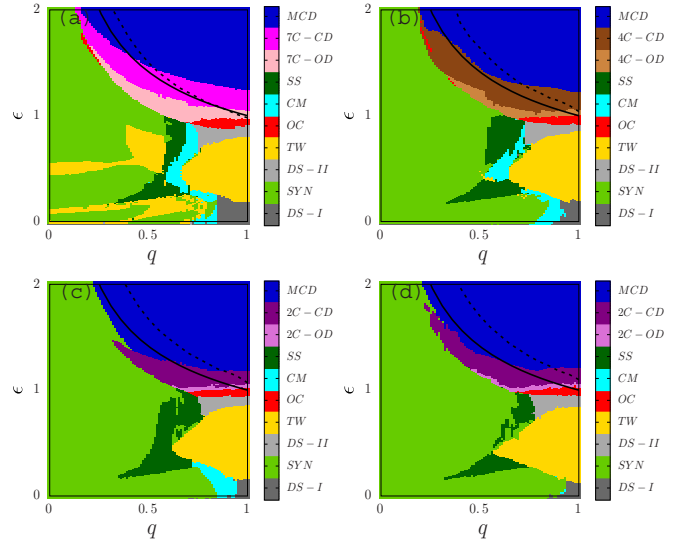

FIG. 11. Two parameter diagrams in (q,ϵ) space for $\alpha = 0.5$ and for the coupling range values (a) $r = 0.1$, (b) $r = 0.2$, (c) $r = 0.3$ and (d) $r = 0.4$. Different colors delineate distinct dynamical regimes. CM, SS, SYN and DS (I and II) represent chimera, solitary, synchronized and desynchronized states (I and II). TW and OC denote traveling wave and oscillatory cluster states. 2C-OD, 4C-OD, and 7C-OD describe two, four and seven cluster oscillation death states. Analogously 2C-CD, 4C-CD, and 7C-CD are the two, four, and seven cluster chimera death states. MCD describes multichimera death state. The dotted line and solid line represent the Floquet stability curve for stable SYN state and linear stability curve for IOD state, respectively.

is observed at very low values of ϵ and traveling waves for larger values of ϵ. Further, transition to desynchronized state (DS-II), oscillatory cluster state (OC), seven cluster oscillation death (7C-OD), seven cluster chimera death (7C-CD) and multichimera death states (MCD) are observed in Fig. 11(a) as a function of the strength of the nonlocal coupling ϵ for $r = 0.1$.

Now, we increase the coupling range r from 0.1 to 0.2 and the corresponding two parameter phase diagram is depicted in Fig. 11(b). Emergence of traveling wave and synchronized state alternately for $r = 0.1$ is suppressed for $r = 0.2$ thereby rendering the oscillators to evolve in complete synchrony for lower values of q and ϵ [see Fig. 11(b)]. One can observe interesting collective dynamics only above a moderate value of q ($q > 0.5$). In this coupling range, similar dynamical behaviors are observed as in Fig. 11(a) for $r = 0.1$ except for the four cluster oscillation death (4C-OD) state and four cluster chimera death (4C-CD) state. Figures 11(c) and 11(d) depict the dynamical behavior for the coupling ranges $r = 0.3$ and $r = 0.4$, respectively. Initially for lower values of q synchronized state is observed for all values of ϵ. At moderate values of q ($q \approx 0.5$), the coupled system exhibits synchronized behavior for lower values of ϵ. There is an excursion of some isolated oscillators away from the synchronized group leading to solitary state for further increase in ϵ. The coupled oscillators exhibit completely synchronized state upon increasing ϵ further. In this region, swing like behavior of synchronized state is observed. At strong coupling limits ($\epsilon >$

1 and $q \approx 0.5$), the coupled oscillators exhibit a steady-state behavior. There is a direct transition from completely synchronized oscillatory state to steady state due to strong trade-off between the attractive and repulsive couplings. By increasing ϵ, traveling wave (TW) state is found to be stable up to $\epsilon \approx 0.8$. Beyond this the oscillators become unstable and the coupled system evolves desynchronously. Further increase in ϵ results in stable homogeneous and inhomogeneous states thereby facilitating oscillatory cluster state (OC). Finally the coupled system attains steady state where all the oscillators reach inhomogeneous state. For the coupling range $r = 0.3$, the two cluster (2C-OD) oscillation death state emerges and becomes two cluster chimera death state as a function of the nonlocal coupling strength ϵ. In 2C-CD state the oscillators in two coherent edges jump between upper and lower inhomogeneous branches facilitating two coherent states and two incoherent states. At strong coupling limits the two cluster chimera death (2C-CD) state becomes a multi-chimera death state (MCD), which is characterized by the emergence of multiple coherent and incoherent branches of steady states. Similar dynamical behaviors are observed in Fig. 11(d) for $r = 0.4$ except for the emergence of chimera state, oscillatory cluster and chimera death states. It is also to be noted that the transition from desynchronized state to chimera death state is always observed through the oscillatory cluster (OC) states for all values of the coupling radius r in contrast to the reports in the literature, where chimera death is observed due to nonisochronicity parameter. In general, complex collective dynamics and their dynamical transitions are observed only for larger values of the repulsive coupling strength $q > 0.5$ elucidating its importance in inducing complex collective dynamics compared with the counter-active attractive coupling.

In addition, incoherent oscillation death state (IOD) coexists with chimera death state in certain regions of parameter space. The analytical boundary of IOD state is deduced from the following linear stability analysis. By distributing the initial state of the oscillators nearly at the inhomogeneous steady state, the system exhibits incoherent oscillation death state. At this IOD state, the system has the following fixed points, $(x_{i-P}, y_{i-P}) = (x_0, y_0),..., (x_{i-2}, y_{i-2}) = (x_0, y_0), (x_{i-1}, y_{i-1}) = (-x_0, -y_0), (x_i, y_i) = (x_0, y_0), (x_{i+1}, y_{i+1}) = (-x_0, -y_0), (x_{i+2}, y_{i+2}) = (x_0, y_0)..., (x_{i+P}, y_{i+P}) = (x_0, y_0)$. By substituting the above-mentioned fixed points in Eq. (1), the system equation can be reduced as

$$y_0 - \beta x_0 = 0,$$
$$\alpha(1 - x_0^2)y_0 - x_0 + q\beta y_0 = 0, \quad (5)$$

where, $\beta = \epsilon$ for even number of nearest neighbors and $\beta = (\frac{P+1}{P})q\epsilon$ for odd number of nearest neighbors. The explicit fixed point solutions for Eq. (5), which can be deduced as

$$x_0 = \pm\sqrt{\frac{-1 + \alpha\beta + q\beta^2}{\alpha\beta}},$$
$$y_0 = \beta x_0. \quad (6)$$

The stability condition can be derived by substituting the fixed points (x_0, y_0) in the $2N \times 2N$ Jacobian matrix of the system

Eq. (1) can be expressed as

$$\mathbf{J} = \begin{pmatrix} a_{11} & a_{12} & a_{13} & a_{14} & \cdots & a_{1N} \\ a_{21} & a_{22} & a_{23} & a_{24} & \cdots & a_{2N} \\ a_{31} & a_{32} & a_{33} & a_{34} & \cdots & a_{3N} \\ a_{41} & a_{42} & a_{43} & a_{44} & \cdots & a_{4N} \\ \vdots & \vdots & \vdots & \vdots & \ddots & \vdots \\ a_{d1} & a_{d2} & a_{d3} & a_{d4} & \cdots & a_{dN} \end{pmatrix}, \quad (7)$$

with $a_{ii} = -\epsilon$, $a_{i(i+1)} = 1$ and $a_{i(i+j+1)} = a_{i(i-j)} = \frac{\epsilon}{2P}$ for $i = 1, 3.., (N-1)$ and $j = 1, 3.., (2P-1)$. Analogously, $a_{i(i-1)} = \gamma_1$, $a_{ii} = \gamma_2$, and $a_{i(i+j)} = a_{i(i-j)} = \frac{-q\epsilon}{2P}$ for $i = 2, 4.., N$ and $j = 2, 4.., 2P$, where $\gamma_1 = 1 - 2\alpha\beta - 2q\beta^2$ and $\gamma_2 = \frac{1}{\beta} - q\beta + q\epsilon$. Here, $a_{i(N+j)} = a_{ij}$ and $a_{i(1-j)} = a_{i(N-j+1)}$ for $j = 1, 2.., P$. From the eigen value analysis conditions for stable IOD region can be obtained [20]. In the stable IOD region the following condition must be satisfied:

$$Tr(J) = \lambda_1 + \lambda_2 + \lambda_3 + ...\lambda_{2N} < 0. \quad (8)$$

For odd and even number of nearest neighbors, the trace of $2N \times 2N$ Jacobian matrix of the considered system can be expressed as

$$\text{Tr}(J) = N(\alpha c_1 - \epsilon\hat{q}) < 0. \quad (9)$$

The following additional condition has also to be satisfied for fixed points to be stable:

$$\det(J) = \lambda_1 \lambda_2 \lambda_3 ... \lambda_{2N} > 0. \quad (10)$$

The stability conditions are found by equating the eigen values of the determinant to zero. In the stable IOD region real parts of all the eigen values acquire negative values. Mainly, the following eigen values play a crucial role in determining the stability,

$$\lambda_1 = \tfrac{1}{4}(2\alpha c_1 \pm \sqrt{(-2\alpha c_1)^2 - 16c2}) \quad (11)$$

$$\lambda_2 = \frac{1}{4P}[2P\alpha c_1 - 6\epsilon\hat{q}$$
$$\pm\sqrt{(-2P\alpha c_1 + 6\epsilon\hat{q})^2 - 16(P^2 c_2 - 3P\alpha\epsilon c_1 - 9q\epsilon^2)}], \quad (12)$$

where $c_1 = (1 - x^2)$ and $c_2 = 1 + 2xy\alpha$ and $\hat{q} = 1 - q$. The stable region emerges at

$$\epsilon_1 = \frac{1}{\sqrt{q}}, \text{ for even } P,$$

$$\epsilon_2 = \left(\frac{P}{P+1}\right)\frac{1}{\sqrt{q}}, \text{ for odd } P,$$

which are obtained from λ_1. The stability condition deduced from λ_1 can be denoted as ϵ_1 and ϵ_2. Similarly, the stability condition deduced from λ_2 can be represented by $\epsilon_3 = [\frac{\epsilon k_2 - 2Pk_1}{\epsilon} + \sqrt{4P(-P - 3\alpha\epsilon + 4k_1) - 36q\epsilon^2 + (\frac{2Pk_1}{\epsilon} - k_2)^2}]$, where $k_1 = -1 + \alpha\epsilon + q\epsilon^2$ and $k_2 = 2P\alpha - 6\epsilon + 6q\epsilon$. The stable IOD region is enclosed by $\epsilon_1 > \frac{1}{\sqrt{q}}$ for $q < 0.65$ and $\epsilon_3 > \frac{-4\alpha + \sqrt{2}\sqrt{25q + 8\alpha^2}}{5\sqrt{q}}$ for $q > 0.65$ $(N = 6, 8, 10, 12.., 100)$. For $P = 2$, the stable region satisfies both the above conditions.
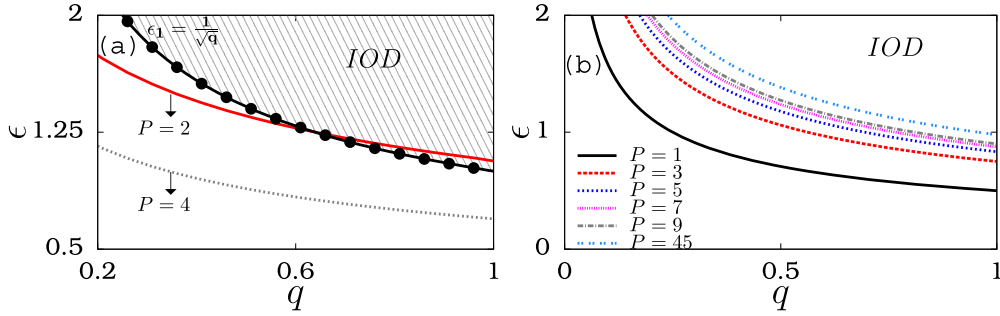
FIG. 12. Boundaries of incoherent oscillation death in (q, ϵ) space for (a) even P and (b) odd P. Stability curves with respect different nearest neighbors are denoted by distinct line types. The shaded region in Figure (a) represents the stable region of IOD state for even number of P.

The corresponding stability curves enclosing the stability regions of IOD state for even number of nearest neighbors is depicted in Fig. 12(a). The solid line and dashed line in Fig. 12(a) represent ϵ_3 at $P = 2$ and $P = 4$, respectively. Comparing both the curves it is clear that for large P, ϵ_3 curve emerges below the stable region. Further for all other even P, the stable region is enclosed only by $\epsilon_1 > \frac{1}{\sqrt{q}}$. The stability curves ϵ_2 enclosing the stable IOD state for odd P's are depicted in Fig. 12(b). The distinct lines correspond to different values of nearest neighbors elucidating that the stable region depends on the number of nearest neighbors. It is to be noted that the stable region decreases with increase in number of nearest neighbors.

The analytical boundary of IOD state is depicted by solid line in all the two parameter diagrams in Fig. 11. The area above the solid line represents the stable IOD region satisfying the stability condition $\epsilon \geqslant \frac{1}{\sqrt{q}}$ for $q \leqslant 1$, which is valid for all even number of nearest neighbors. It is to be noted that the above stability condition is the same as that of the two coupled network as it repeats for N-coupled network with even number of nearest neighbors.

Finally, the area under the dashed line in all the two phase diagrams denote stable regions of synchronized state, which is confirmed using Floquet exponents from Eq. (4). The stable synchronized oscillations coexists with SS, TW, CM, DS-I, DS-II, and OC states. The synchronized state also coexists with coherent oscillation death and chimera death states in certain ranges of parameters. The stability

curves of synchronized states are shown separately in Fig. 13, where the four different line points represent the four distinct coupling radius $r = 0.1, 0.2, 0.3,$ and 0.4. The stability of synchronized state was also verified through master stability function [54,55].

VI. CONCLUSIONS

In summary, we have investigated the emergence of chimera death states in a network of nonlocally coupled van der Pol oscillators due to the combined effect of both the attractive and repulsive couplings. We found that the repulsive coupling plays a crucial role in inducing various collective dynamics. In particular, we have shown that the chimera death state emerges through a novel transition route, namely, oscillatory cluster state (OC) due to strong trade-off between the attractive and repulsive couplings. It is also shown that the network of coupled vdP oscillators takes the same transition route in all the coupling ranges. Strong competing interaction between the couplings renders the oscillators either in homogeneous or inhomogeneous oscillatory states. We have also elucidated that an increase in the coupling radius leads to a decrease in the number of clusters (coherent states) and increases the cluster size (coherent regions). Finally, we have observed that increase in coupling strength leads to structural changes in coherent death state and to the transition from coherent oscillation death to multichimera death via distinct cluster chimera death state. Furthermore, the coexistence of incoherent death state is also found to coexist with the chimera death state and the corresponding analytical stability was deduced. Analytical stability curves for the synchronized and solitary states were also deduced.
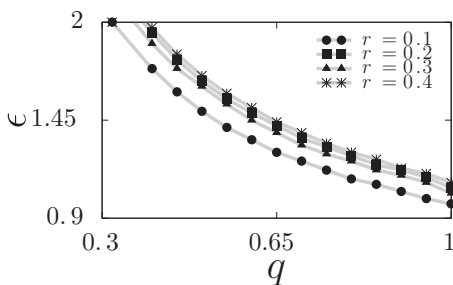
FIG. 13. Boundaries of stable completely synchronized state for four distinct coupling ranges in (q, ϵ) space. Different line points such as circle, rectangle, triangle and star points with line represent coupling ranges $r = 0.1, r = 0.2, r = 0.3$ and $r = 0.4$, respectively.

[1] A. Pikovsky, M. G. Rosenblum, and J. Kurths, *Synchronization: A Universal Concept in Nonlinear Sciences* (Cambridge University Press, Cambridge, 2001).

[2] W. Zou, D. V. Senthilkumar, R. Nagao, I. Z. Kiss, Y. Tang, A. Koseska, J. Duan, and J. Kurths, Nat. Commun. **6**, 7709 (2015)

[3] D. G. Aronson, G. B. Ermentrout, and N. Koppel, Physica D **41**, 403 (1990).

[4] P. C. Matthews and S. H. Strogatz, Phys. Rev. Lett. **65**, 1701 (1990); P. C. Matthews, R. E. Mirollo, and S. H. Strogatz, Physica D **52**, 293 (1991).

[5] A. Sharma and M. D. Shrimali, Phys. Rev. E **85**, 057204 (2012).

[6] A. Koseska, E. I. Volkov, A. Zaikin, and J. Kurths, Phys. Rev. E **75**, 031916 (2007).

[7] D. V. Ramana Reddy, A. Sen, and G. L. Johnston, Phys. Rev. Lett. **80**, 5109 (1998).

[8] I. Prigogine and R. Lefever, J. Chem. Phys. **48**, 1695 (1968); A. Koseska, E. Volkov, and Kurths, J. Phys. Rep. **531**, 173 (2013).

[9] W. Zou, D. V. Senthilkumar, Y. Tang, and J. Kurths, Phys. Rev. E **86**, 036210 (2012).

[10] W. Zou, D. V. Senthilkumar, J. Duan, and J. Kurths, Phys. Rev. E **90**, 032906 (2014).

[11] K. Konishi, Phys. Rev. E **68**, 067202 (2003).

[12] R. Karnatak, R. Ramaswamy, and A. Prasad, Phys. Rev. E **76**, 035201(R) (2007).

[13] V. Resmi, G. Ambika, and R. E. Amritkar, Phys. Rev. E **84**, 046212 (2011).

[14] C. R. Hens, O. I. Olusola, P. Pal, and S. K. Dana, Phys. Rev. E **88**, 034902 (2013).

[15] E. Ullner, A. Zaikin, E. I. Volkov, and J. Garcia-Ojalvo, Phys. Rev. Lett. **99**, 148103 (2007).

[16] M. F. Crowley and I. R. Epstein, J. Phys. Chem. **93**, 2496 (1989).

[17] M. Toiya, V. K. Vanag, and I. R. Epstein, Angew. Chem., Int. Ed. **47**, 7753 (2008).

[18] K. P. Zeyer, M. Mangold, and E. D. Gilles, J. Phys. Chem. A **105**, 7216 (2001).

[19] M. Heinrich, T. Dahms, V. Flunkert, S. W. Teitsworth, and E. Schöll, New J. Phys. **12**, 113030 (2010).

[20] A. Mishra, S. Saha, P. K. Roy, T. Kapitaniak, and S. K. Dana, Chaos **27**, 023110 (2017).

[21] Y. Kuramoto and D. Battogtokh, Nonlinear Phenom. Complex Syst. **5**, 380 (2002).

[22] D. M. Abrams and S. H. Strogatz, Phys. Rev. Lett. **93**, 174102 (2004).

[23] D. M. Abrams and S. H. Strogatz, Int. J. Bif. Choas **16**, 21 (2006).

[24] M. J. Panaggio and D. M. Abrams, Nonlinearity **28**, R67 (2015).

[25] I. Omelchenko, A. Provata, J. Hizanidis, E. Schöll, and P. Hövel, Phys. Rev. E **91**, 022917 (2015).

[26] T. Banerjee, P. S. Dutta, A. Zakharova, and E. Schöll, Phys. Rev. E **94**, 032206 (2016).

[27] I. Omelchenko, Y. Maistrenko, P. Hövel, and E. Schöll, Phys. Rev. Lett. **106**, 234102 (2011).

[28] V. Semenov, A. Feoktistov, T. Vadivasova, E. Schöll, and A. Zakharova, Chaos **25**, 033111 (2015).

[29] R. Gopal, V. K. Chandrasekar, A Venkatesan, and M Lakshmanan, Phys. Rev. E **89**, 052914 (2014).

[30] K. Kaneko, Physica D **41**, 137 (1990); Chaos **25**, 097608 (2015); A. Yeldesbay, A. Pikovsky, and M. Rosenblum, Phys. Rev. Lett. **112**, 144103 (2014); G. C. Sethia and A. Sen, *ibid.* **112**, 144101 (2014).

[31] V. K. Chandrasekar, R. Gopal, A. Venkatesan, and M. Lakshmanan, Phys. Rev. E **90**, 062913 (2014).

[32] A. Mishra, C. Hens, M. Bose, P. K. Roy, and S. K. Dana, Phys. Rev. E **92**, 062920 (2015).

[33] B. K. Bera, D. Ghosh, and M. Lakshmanan, Phys. Rev. E **93**, 012205 (2016).

[34] C. R. Laing, Phys. Rev. E **92**, 050904(R) (2015).

[35] B. K. Bera and D. Ghosh, Phys. Rev. E **93**, 052223 (2016).

[36] B. K. Bera, D. Ghosh, and T. Banerjee, Phys. Rev. E **94**, 012215 (2016).

[37] N. C. Rattenborg, C. J. Amlaner, and S.L. Lima, Neurosci. Biobehav. Rev. **2**, 817 (2000).

[38] A. Rothkegel and K. Lehnertz, New J. Phys. **16**, 055006 (2014).

[39] C. R. Laing and C. C. Chow, Neural Comput. **13**, 1473 (2001).

[40] H. Sakaguchi, Phys. Rev. E **73**, 031907 (2006).

[41] A. E. Filatova, A. E. Hramov, A. A. Koronovskii, and S. Boccaletti, Chaos **18**, 023133 (2008).

[42] J. C. Gonz alez-Avella, M. G. Cosenza, and M. San Miguel, Physica A **399**, 24 (2014).

[43] A. Zakharova, M. Kapeller, and E. Schöll, Phys. Rev. Lett. **112**, 154101 (2014).

[44] A. Zakharova, M. Kapeller, and E. Schöll, IOP Publishing, Conference Series **727**, 012018 (2016).

[45] L. Tumash, A. Zakharova, J. Lehnert, W. Just, and E. Schöll, Europhys. Lett. **117**, 20001 (2017).

[46] K. Premalatha, V. K. Chandrasekar, M. Senthilvelan, and M. Lakshmanan, Phys. Rev. E **93**, 052213 (2016).

[47] K. Premalatha, V. K. Chandrasekar, M. Senthilvelan, and M. Lakshmanan, Phys. Rev. E **91**, 052915 (2015).

[48] Z. Qu, Y. Shiferaw, and J. N. Weiss, Phys. Rev. E **75**, 011927 (2007).

[49] T. Yanagita, T. Ichinomiya, and Y. Oyama, Phys. Rev. E **72**, 056218 (2005).

[50] Xiao-Jun Tian, Xiao-Peng Zhang, F. Liu, and W. Wang, Phys. Rev. E **80**, 011926 (2009)

[51] J. Guckenheimer, K. Hoffman, and W. Weckesser, Numerical computation of canards, Int. J. Bifurcat. Chaos Appl. Sci. Eng. **10**, 2669 (2000).

[52] P. F. Rowat and A. I. Selverston, Modeling the gastric mill central pattern generator of the lobsterwith a relaxation-oscillator network, J. Neurophysiol. **70**, 1030 (1993).

[53] H. Daido and K. Nakanishi, Phys. Rev. Lett. **96**, 054101 (2006).

[54] L. M. Pecora and T. L. Carroll, Phys. Rev. Lett. **80**, 2109 (1998).

[55] V. K. Chandrasekar, R. Gopal, D. V. Senthilkumar, and M. Lakshmanan, Phys. Rev. E **94**, 012208 (2016).